PHYSICAL REVIEW C **76**, 064601 (2007)

Formation of the isomeric pairs $^{139}Nd^{m,g}$ and $^{141}Nd^{m,g}$ in proton and ^{3}He-particle-induced nuclear reactions

K. Hilgers,[1] S. Sudár,[1,2] and S. M. Qaim[1,*]
[1]*Institut für Nuklearchemie, Forschungszentrum Jülich, D-52425 Jülich, Germany*
[2]*Institute of Experimental Physics, University of Debrecen, Bem tér 18/a, H-4026 Debrecen, Hungary*
(Received 22 August 2007; published 4 December 2007)

Cross sections were measured by the activation technique for the nuclear reactions $^{141}Pr(p,n)^{141}Nd^{m}$, $^{141}Pr(p,3n)^{139}Nd^{m}$, $^{nat}Ce(^{3}He,xn)^{141}Nd^{m}$, and $^{nat}Ce(^{3}He,xn)^{139}Nd^{m}$ up to proton energies of 44 MeV and ^{3}He-particle energies of 35 MeV. Using the present data and some of our earlier experimental results the isomeric cross-section ratios for the nuclide pairs $^{139}Nd^{m,g}$ and $^{141}Nd^{m,g}$ were calculated. The experimental data were compared with the results of nuclear model calculations using the code STAPRE, which combines the statistical and precompound formalisms. In general the experimentally determined excitation functions as well as the isomeric cross-section ratios could be described by the theory within the limits of experimental uncertainties, but using relatively low values of η [i.e., the ratio of the effective moment of inertia to the rigid-body moment of inertia ($\Theta_{eff}/\Theta_{rig}$)]. The mass dependence of η could be confirmed.

DOI: 10.1103/PhysRevC.76.064601 PACS number(s): 24.10.−i, 25.40.−h, 27.60.+j, 24.60.Dr

I. INTRODUCTION

Studies of isomeric cross sections are of considerable fundamental interest. It is known that the isomeric cross-section ratio is governed primarily by the spins of the levels involved, rather than by their separation energies [1,2]. Through detailed investigations on the formation of several isomeric pairs, such as $^{58}Co^{m,g}$, $^{73}Se^{m,g}$, $^{94}Tc^{m,g}$, and $^{120}I^{m,g}$, involving different combinations of target, projectile, and ejectile, the effects of changes in the ratio of the effective moment of inertia to the rigid-body moment of inertia ($\eta = \Theta_{eff}/\Theta_{rig}$), assumptions regarding the angular momentum distribution after pre-equilibrium (PE) decay, and the role of input nuclear structure information have been elucidated [1–5]. Furthermore, in two recent studies [6,7] dealing with the high-spin isomers $^{195}Hg^{m}$ and $^{197}Hg^{m}$ it has been suggested that the η value is mass dependent. Now we report on the formation of the isomeric pairs $^{141}Nd^{m,g}$ and $^{139}Nd^{m,g}$ in proton and ^{3}He-particle-induced reactions because very few isomeric pairs in this mass region have been investigated. The low-lying isomeric levels of the two nuclides are shown in Fig. 1. In each case the ground state has a low spin ($3/2^{+}$) and the metastable state a higher spin ($11/2^{-}$).

Experimental and theoretical studies on the total formation cross sections were reported earlier [8]. The experimental excitation functions for both proton and ^{3}He-particle-induced reaction were reproduced well by the nuclear model calculations using the precompound hybrid code ALICE-IPPE [8].

The present work deals primarily with the formation of the isomeric states and a theoretical interpretation of their cross-section ratios.

II. EXPERIMENT

A. Samples, irradiations, and beam-current monitoring

The experimental techniques pertinent to the measurement of total reaction cross sections ($m + g$) of the processes leading to the formation of ^{139,140,141}Nd in proton-induced reactions on ^{141}Pr and in ^{3}He-particle-induced reactions on ^{nat}Ce have been recently described in detail [8]. In the present work dealing with the formation of the metastable states the techniques of sample preparation were the same. Thin samples of CeO_2 and Pr_2O_3 of natural isotopic composition and high chemical purity (99.999%, Koch-Light Laboratories, UK) were prepared by sedimentation on 25 μm thick Cu foils, which were then covered by 10 μm thick Al foils. Irradiations were done in two different ways. While investigating the short-lived $^{141}Nd^{m}$ ($T_{1/2} = 62$ s), each time a single sample, together with a Cu monitor foil, was irradiated. The primary proton energies used were 20, 16, and 12 MeV and several Al absorbers were placed in front of each sample to obtain a different effective projectile energy for each sample. In case of irradiations with ^{3}He particles, the primary ^{3}He-particle energies used were 36 and 25 MeV and a few Ti foils were used as monitors. Again appropriate absorbers were used to obtain different effective projectile energies in various samples. All those irradiations were done at the compact cyclotron CV28 of the Forschungszentrum (FZ) Jülich, Germany. In contrast to the short-lived $^{141}Nd^{m}$, the longer lived $^{139}Nd^{m}$ ($T_{1/2} = 5.5$ h) was studied via the conventional stacked-foil technique [6,8]. About five samples and several absorbers and monitor foils were put together in a stack and irradiated simultaneously. The investigated proton energy range was extended up to 44 MeV. Irradiations covering the proton energy range up to 20 MeV were done at the CV28, and beyond 20 MeV at the injector of COSY at FZ Jülich. The beam current used in each irradiation was about 100 nA; it was measured via the $^{63}Cu(p,xn)^{62,65}Zn$ or $^{nat}Ti(^{3}He,x)^{48}V$ processes. The cross sections of those monitor reactions were taken from the evaluated data file [9].

*Corresponding author: s.m.qaim@fz-juelich.de

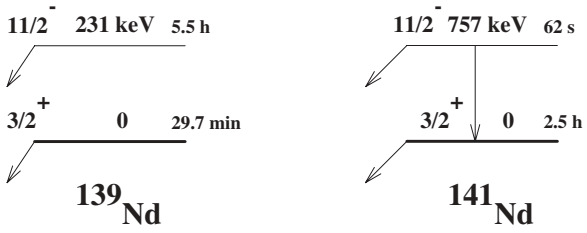

FIG. 1. Level schemes of the isomeric pairs $^{141}Nd^{m,g}$ and $^{139}Nd^{m,g}$.

B. Measurement of radioactivity

For measurement of radioactivity, in each case a HPGe detector was used and the γ-ray spectrum recorded several times to check the half-life of the product. In the case of $^{141}Nd^{m}$ ($T_{1/2} = 62$ s), the activity was measured immediately after the irradiation. A typical γ-ray spectrum is shown in Fig. 2. The characteristic γ-ray peak at 757 keV ($I_\gamma = 91.5\%$) was clearly discernible, though the statistics was not very good. Measurement on the $^{139}Nd^{m}$ ($T_{1/2} = 5.5$ h) was done using the 708-keV ($I_\gamma = 26.0\%$) and 738-keV ($I_\gamma = 35.08\%$) γ rays about 5 h after the end of each irradiation to allow the shorter lived radionuclides to decay. A typical γ-ray spectrum, taken at about 7.5 h after end of bombardment (EOB), is reproduced in Fig. 3. It is relatively clean and the γ rays of $^{139}Nd^{m}$ are clearly visible. In general, the samples were placed at a distance of at least 10 cm from the detector to avoid coincidence losses. The detectors were calibrated with standard sources supplied by the Physikalische Technische Bundesanstalt (PTB) and Amersham International. The decay data of the isomeric states under investigation were taken from the Tables of Isotopes [10]. The absolute activity was derived by applying the usual corrections such as those for γ-ray intensity and detector efficiency.

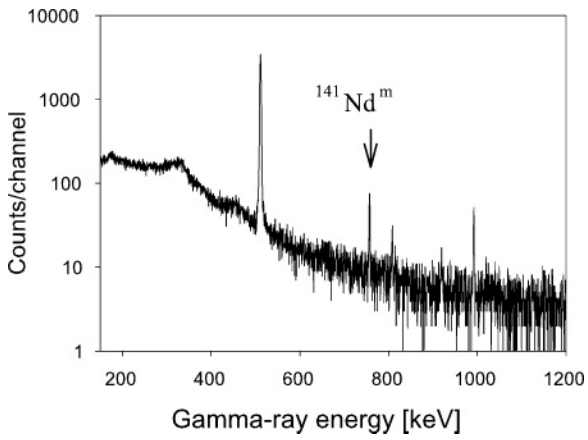

FIG. 2. Gamma-ray spectrum of $^{nat}CeO_2$ sample irradiated with 18.3-MeV ^{3}He particles for 2 minutes; spectrum recorded at 2 min after end of bombardment, with a counting time of 30 s. The 757-keV peak of $^{141}Nd^{m}$ was clearly visible; its intensity decreased with a half-life of 62 ± 2 s.

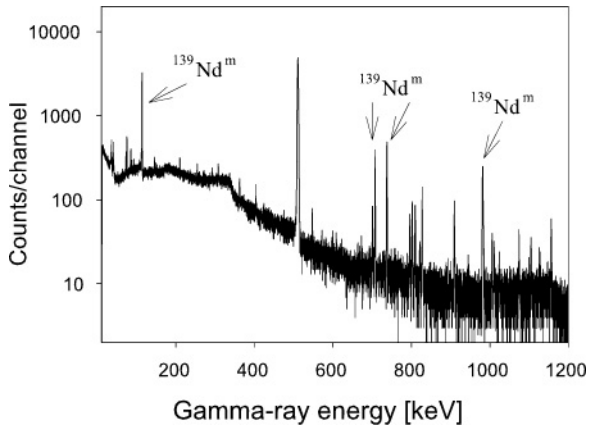

FIG. 3. Gamma-ray spectrum of $^{nat}CeO_2$ sample irradiated with 29.1-MeV ^{3}He particles for 60 min; spectrum recorded for 1 h at 7.5 h after EOB. The spectrum is relatively clean and the peaks at 114, 708, 738, and 982 keV, characteristic of $^{139}Nd^{m}$, are clearly visible. The intensities of the peaks decreased with a half-life of 5.5 ± 0.2 h.

C. Calculation of cross sections, isomeric cross-section ratios, and relevant uncertainties

From the beam flux and the reaction product activity, the cross section was calculated by using the activation equation. Uncertainties were estimated as described earlier [8]. The total uncertainty in each cross section was 15–20%. The isomeric cross-section ratio [σ_m/σ_g or $\sigma_m/(\sigma_g + \sigma_m)$] for each pair was then calculated by using the experimentally determined cross-section values. The uncertainty in each isomeric cross-section ratio amounted to about 25%.

III. NUCLEAR MODEL CALCULATIONS

Cross sections were calculated with the code STAPRE [11], which employs the Hauser-Feshbach formalism for the equilibrium emission and the exciton model for the PE emission. Previously, this code has been used very successfully for calculating isomeric cross sections [2–7]. The transmission coefficients for neutrons, protons, deuterons, ^{3}He, and α particles were provided as input data to the code by means of the spherical optical code SCAT-2 [12] using global parameter sets. For the neutron and ^{3}He the optical model parameter set of Becchetti and Greenlees [13] was used and for the proton and deuteron those of Perey [14] were used. In the case of α particles, a modified set of optical model parameters of McFadden and Satchler [15] was used. For the energy and mass dependence of the effective matrix element ($|M|^2$) of the internal transition, the $|M|^2 = (FM)\cdot A^{-3}E^{-1}$ formula was applied. The energies, spins, parities, and branching ratios of the discrete levels were obtained from the NNDC On-Line Data Service of the ENSDF database [16]. In cases where the spin and parity were not known, estimates from adjacent levels were made. In the continuum region the level density was calculated by the back-shifted Fermi gas (BSFG) formula [17] and the level density parameter given in Refs. [17,18]. The level density parameter (a) for the calculation was selected by interpolating the data of the neighboring isotopes, taking into

TABLE I. Measured cross sections of the ^{141}Pr$(p, n)^{141}$Nd^m reaction.

Particle energy (MeV)	Cross section (mb)
9.0±0.4	56±8
9.6±0.4	71±11
10.3±0.4	104±16
10.8±0.3	110±17
11.3±0.3	136±20
12.4±0.4	196±29
12.7±0.4	193±29
13.3±0.3	169±25
14.3±0.3	210±32
15.6±0.3	51±8

account the odd-even systematics. The back-shift parameter (Δ) was determined individually for all nuclei used in the model calculation. The cumulative plot of the known discrete levels, collected from the ENSDF database, was fitted by the BSFG formula while the level spacing at the neutron binding energy was kept according to the experimental value. The spin distribution of the level density was characterized by the ratio (η) of the effective moment of inertia Θ_{eff} to the rigid-body moment of inertia Θ_{rig} ($\eta = \Theta_{\text{eff}}/\Theta_{\text{rig}}$) and the calculations were performed for different η values to find the best agreement with the experimental data. The transmission coefficients of photons are also of considerable significance in calculations on isomeric cross sections. They were derived from the γ-ray strength functions. For the $E1$ transition the Brink-Axel model with global parameters was applied, whereas for the $M1$, $E2$, $M2$, $E3$, and $M3$ radiation the Weisskopf model was used.

IV. RESULTS AND DISCUSSION

A. Experimental cross-section data

The measured cross sections for the nuclear reactions ^{141}Pr$(p, n)^{141}$Nd^m, ^{141}Pr$(p, 3n)^{139}$Nd^m, $^{\text{nat}}$Ce$(^3$He$, xn)^{141}$Nd^m, and $^{\text{nat}}$Ce$(^3$He$, xn)^{139}$Nd^m are given in Tables I–IV. The overall uncertainties amount to about 15–30%. Almost all the data have been measured for the first time. Some relevant nuclear data were also measured in a broader collaboration among Cape Town, Los Alamos, Debrecen, and Jülich [19].

TABLE II. Measured cross sections of the ^{141}Pr$(p, 3n)^{139}$Nd^m reaction.

Particle energy (MeV)	Cross section (mb)
21.0±1.0	0.6±0.1
25.3±0.8	235±22
26.6±0.7	337±35
29.5±0.7	457±39
30.4±0.7	514±75
32.9±0.6	603±28
39.1±0.4	328±49
41.6±0.3	324±49
43.8±0.3	132±20
44.8±0.3	239±36

TABLE III. Measured cross sections of the $^{\text{nat}}$Ce$(^3$He$, xn)^{141}$Nd^m reaction.

Particle energy (MeV)	Cross section (mb)
18.3±0.5	82±25
19.4±0.5	85±26
20.7±0.4	97±13
22.1±0.4	103±31
22.9±0.4	61±18
23.3±0.4	90±27
24.5±0.3	123±37
25.6±0.5	68±20
26.5±0.5	76±23
28.1±0.4	81±24
29.2±0.4	95±29
30.3±0.4	94±28
31.3±0.4	96±29
32.3±0.3	93±28
34.2±0.3	54±16

B. Excitation functions

The cross sections for the nuclear reactions ^{141}Pr$(p, n)^{141}$Nd^m, ^{141}Pr$(p, n)^{141}$Nd^{m+g}, ^{141}Pr$(p, 3n)^{139}$Nd^m, ^{141}Pr$(p, 3n)^{139}$Nd^g, $^{\text{nat}}$Ce$(^3$He$, xn)^{141}$Nd^m, $^{\text{nat}}$Ce$(^3$He$, xn)^{141}$Nd^{m+g}, $^{\text{nat}}$Ce$(^3$He$, xn)^{139}$Nd^m, and $^{\text{nat}}$Ce$(^3$He$, xn)^{139}$Nd^g are shown as a function of the projectile energy in Figs. 4–11. The data for the metastable states have been determined in this work whereas the total cross section ($m + g$) for each channel was measured earlier [8]. For the ^{141}Pr$(p, 3n)^{139}$Nd^m ($T_{1/2} = 5.5$ h), ^{141}Pr$(p, 3n)^{139}$Nd^g ($T_{1/2} = 29.7$ min), and ^{141}Pr$(p, n)^{141}$Nd^{m+g} reactions some literature data were available [19]; they are also shown in the respective figures, and they generally agree well with our data. The shapes of excitation functions of the reactions $^{\text{nat}}$Ce$(^3$He$, xn)^{141}$Nd^m (Fig. 8) and $^{\text{nat}}$Ce$(^3$He$, xn)^{141}$Nd^{m+g} (Fig. 9) are somewhat flat at energies above 22 MeV. This is due to the two contributing processes, namely ^{140}Ce$(^3$He$, 2n)^{141}$Nd^{m,g}

TABLE IV. Measured cross sections of the $^{\text{nat}}$Ce$(^3$He$, xn)^{139}$Nd^m reaction.

Particle energy (MeV)	Cross section (mb)
27.7±0.5	5±2
29.1±0.4	50±15
30.5±0.4	55±17
32.0±0.3	283±85
33.2±0.3	128±39
33.8±0.3	215±64
35.2±0.3	376±113

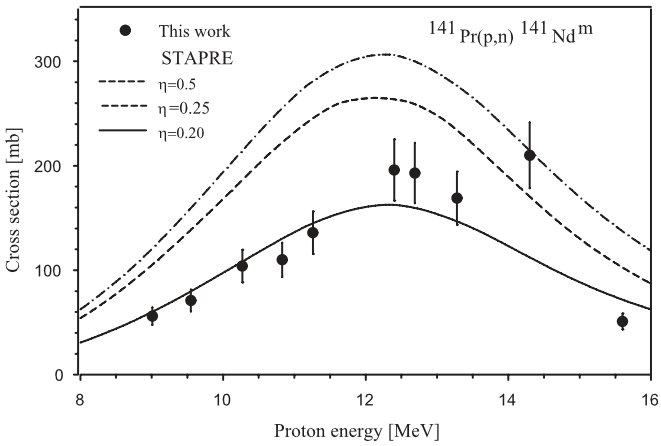

FIG. 4. Measured and calculated excitation function of the ^{141}Pr(p, n)^{141}Nd^{m} reaction.

and ^{142}Ce(^{3}He, $4n$)^{141}Nd^{m,g}. Similarly in the case of ^{nat}Ce(^{3}He, xn)^{139}Nd^{m,g} reactions (Figs. 10 and 11) the data shown cover only the increasing parts of the excitation functions of the high-threshold ^{140}Ce(^{3}He, $4n$)^{139}Nd^{m,g} processes.

The results of nuclear model calculations are given in Figs. 4–11 together with the experimental data. In the case of the ^{141}Pr(p, n)^{141}Nd^{m} reaction (Fig. 4), the effect of increasing η is shown. Evidently the theoretical curve is strongly dependent on the η value. The best fit is obtained while using a small η value of about 0.20. In contrast, the ^{141}Pr(p, n)^{141}Nd^{m+g} reaction (Fig. 5; i.e., the summed cross section of the reaction channel under consideration) is relatively independent of the η value. In all the other cases, in general, the experimentally determined excitation functions are reproduced by the theory within the limits of experimental uncertainties. It should be pointed out that the best theoretical fit to the experimental data for each reaction channel was obtained while using a low η value of 0.20 to 0.25.

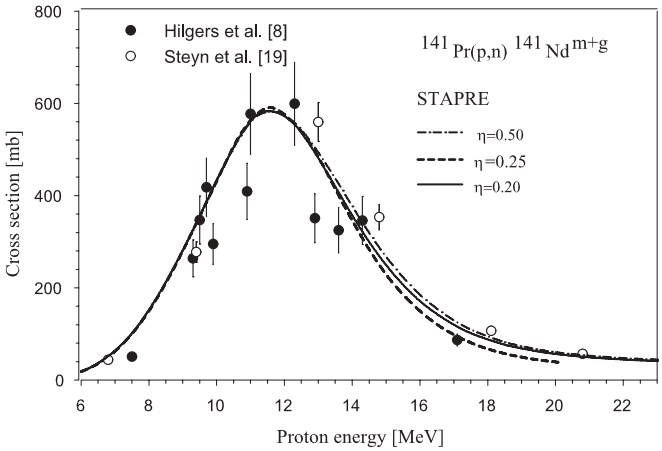

FIG. 5. Measured and calculated excitation function of the ^{141}Pr(p, n)^{141}Nd^{m+g} reaction.

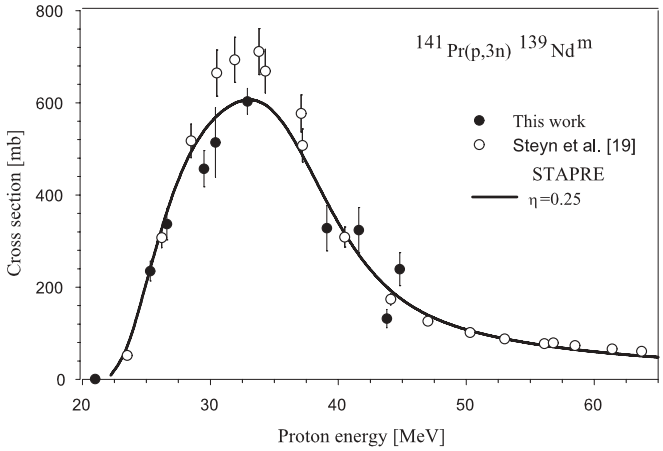

FIG. 6. Measured and calculated excitation function of the ^{141}Pr(p, $3n$)^{139}Nd^{m} reaction.

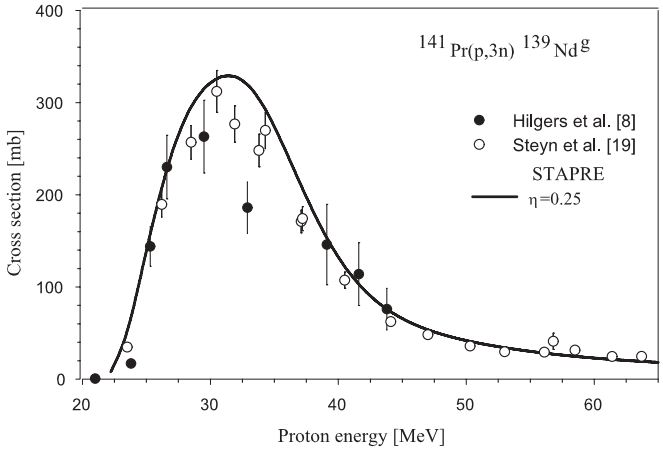

FIG. 7. Measured and calculated excitation function of the ^{141}Pr(p, $3n$)^{139}Nd^{g} reaction.

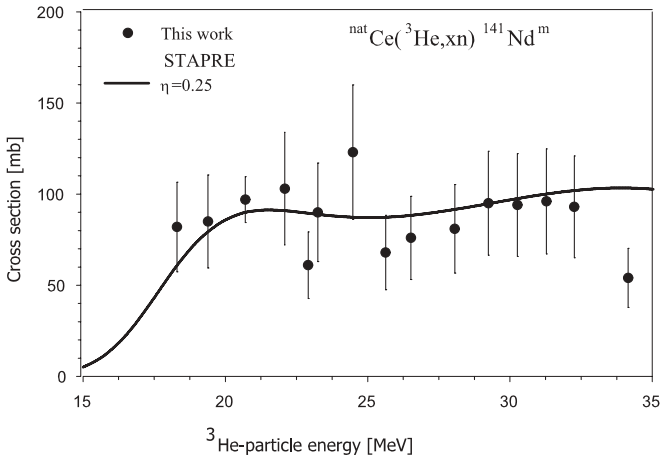

FIG. 8. Measured and calculated excitation function of the ^{nat}Ce(^{3}He, xn)^{141}Nd^{m} reaction.

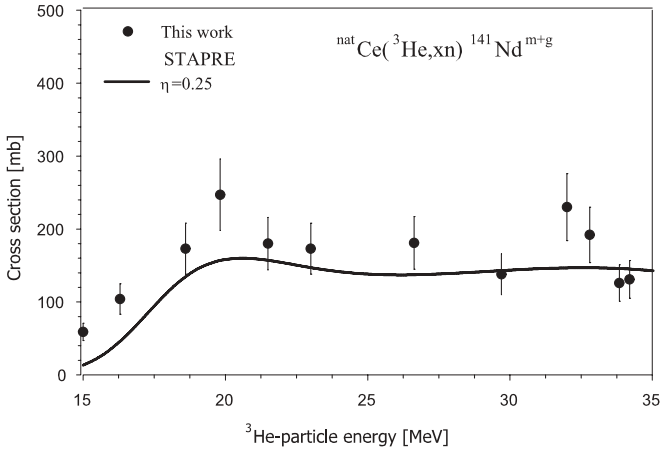

FIG. 9. Measured and calculated excitation function of the ^{nat}Ce(^{3}He, xn)^{141}Nd^{m+g} reaction.

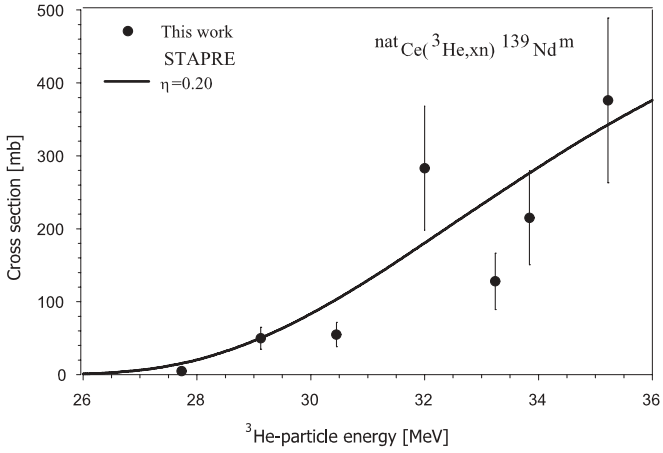

FIG. 10. Measured and calculated excitation function of the ^{nat}Ce(^{3}He, xn)^{139}Nd^{m} reaction.

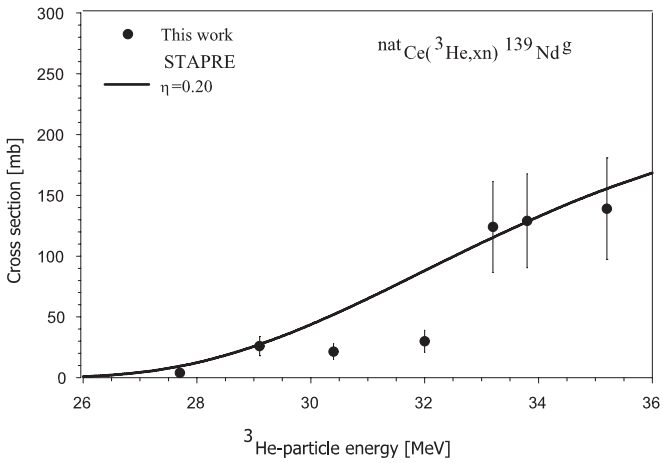

FIG. 11. Measured and calculated excitation function of the ^{nat}Ce(^{3}He, xn)^{139}Nd^{g} reaction.

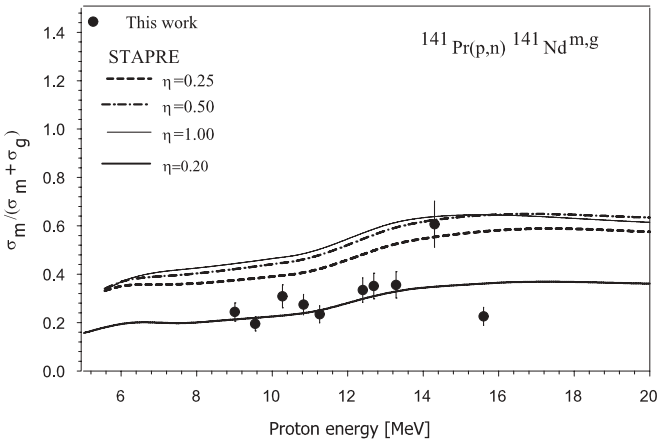

FIG. 12. Measured and calculated isomeric cross-section ratio of the ^{141}Pr(p, n)^{141}Nd^{m,g} reaction, plotted as a function of the projectile energy.

C. Isomeric cross-section ratios

The experimentally measured and theoretically calculated isomeric cross-section ratios for the radionuclide pairs ^{141}Nd^{m,g} and ^{139}Nd^{m,g} in proton- and ^{3}He-particle-induced reactions are shown in Figs. 12–15. For the pair ^{141}Nd^{m,g} the ratio $\sigma_m/(\sigma_m + \sigma_g)$ is plotted against the projectile energy because $(\sigma_m + \sigma_g)$ was measured after the complete decay of the metastable state to the ground state (Figs. 12 and 14). However, for the pair ^{139}Nd^{m,g} the ratio σ_m/σ_g is plotted against the projectile energy because both σ_m and σ_g were measured independently (Figs. 13 and 15). The ratio is relatively low in the case of ^{141}Nd^{m,g} (Figs. 12 and 14), increasing slightly with the increasing projectile energy. For the pair ^{139}Nd^{m,g} (Figs. 13 and 15) the ratio is somewhat higher but the increase with increasing projectile energy is not very pronounced.

As far as a comparison of the experimental data with the theory is concerned the agreement appears to be at extreme limits of experimental uncertainties. The effect of the varying

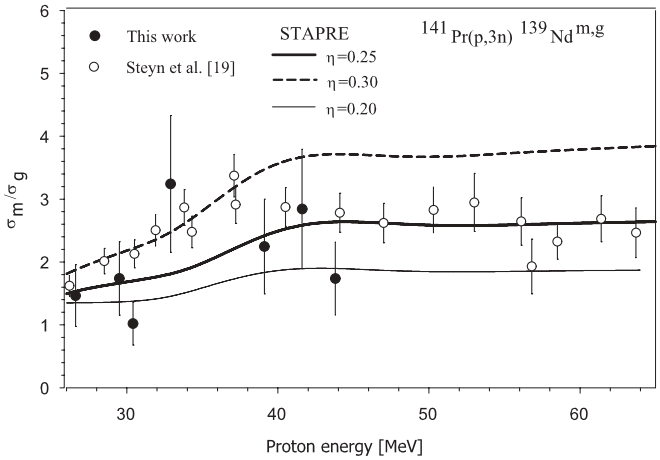

FIG. 13. Measured and calculated isomeric cross-section ratio of the ^{141}Pr(p, $3n$)^{139}Nd^{m,g} reaction, plotted as a function of the projectile energy.

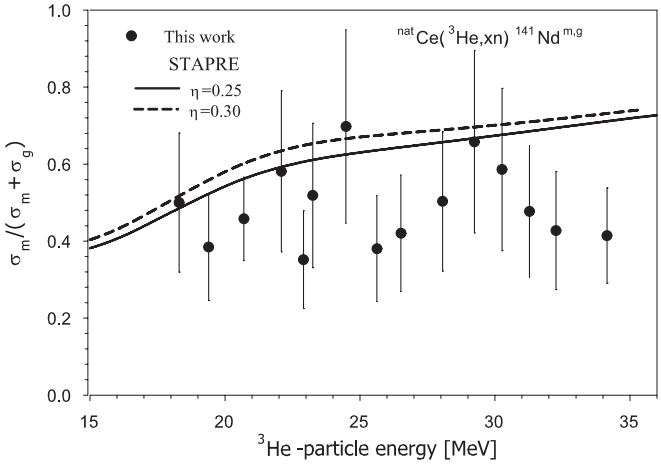

FIG. 14. Measured and calculated isomeric cross-section ratio of the ^{nat}Ce(^{3}He, xn)^{141}Nd^{m,g} reaction, plotted as a function of the projectile energy.

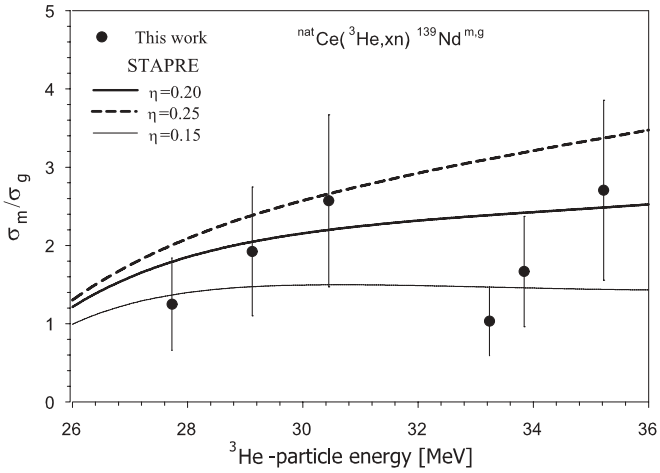

FIG. 15. Measured and calculated isomeric cross-section ratio of the ^{nat}Ce(^{3}He, xn)^{139}Nd^{m,g} reaction, plotted as a function of the projectile energy.

η value, however, is more pronounced for the pair ^{139}Nd^{m,g} than for the pair ^{141}Nd^{m,g}. Whereas all the measured ratios for ^{139}Nd^{m,g} can be encompassed using η values in the range of 0.15 to 0.30 (Figs. 13 and 15), for the pair ^{141}Nd^{m,g} the calculated isomeric cross-section ratios are relatively less sensitive to the η value. However, in the latter case also the low η value appears to be more favorable. It may be mentioned that the pair ^{141}Nd^{m,g} is formed in relatively low energy reactions (with thresholds of about 7 and 14 MeV), whereas the pair ^{139}Nd^{m,g} is formed in higher energy reactions (with thresholds of about 22 and 27 MeV). The estimated η values for ^{141}Nd^{m,g} and ^{139}Nd^{m,g} are $\eta = 0.23 \pm 0.07$ and $\eta = 0.22 \pm 0.07$, respectively. The present results thus lead to the conclusion that the previously postulated mass dependence of η [6] is valid, showing that η values lower than 0.5 are needed to explain the isomeric cross-section ratios even for lighter mass radionuclide pairs than ^{195}Hg^{m,g} and ^{197}Hg^{m,g} isomers.

ACKNOWLEDGMENTS

We thank Prof. H. H. Coenen and Prof. J. Csikai for their kind support of this project, the crews of the compact cyclotron CV 28 and injector of COSY for performing the irradiations, and S. Spellerberg for some experimental assistance.

[1] S. M. Qaim, A. Mushtaq, and M. Uhl, Phys. Rev. C **38**, 645 (1988).
[2] F. Cserpák, S. Sudár, J. Csikai, and S. M. Qaim, Phys. Rev. C **49**, 1525 (1994).
[3] S. Sudár and S. M. Qaim, Phys. Rev. C **53**, 2885 (1996).
[4] B. Strohmaier, M. Fassbender, and S. M. Qaim, Phys. Rev. C **56**, 2654 (1997).
[5] S. Sudár, A. Hohn, and S. M. Qaim, Appl. Radiat. Isotopes **52**, 937 (2000).
[6] S. Sudár and S. M. Qaim, Phys. Rev. C **73**, 034613 (2006).
[7] M. Al-Abyad, S. Sudár, M. N. H. Comsan, and S. M. Qaim, Phys. Rev. C **73**, 064608 (2006).
[8] K. Hilgers, Y. N. Shubin, H. H. Coenen, and S. M. Qaim, Radiochim. Acta **93**, 553 (2005).
[9] F. Tárkányi, S. Takács, K. Gul, A. Hermanne, M. G. Mustafa, F. M. Nortier, P. Oblozinsky, S. M. Qaim, B. Scholten, Y. Shubin, *et al.*, in *Charged-Particle Cross Section Database for Medical Radioisotope Production* (International Atomic Energy Agency, Vienna, 2001), IAEA-TECDOC-1211, p. 49.
[10] R. B. Firestone, *Table of Isotopes*, CDROM Ed. Version 1.0 (Wiley-Interscience, New York, 1996).
[11] M. Uhl and B. Strohmaier, in *Computer Code for Particle Induced Activation Cross Section and Related Quantities* (Institut für Radiumforschung und Kernphysik, Vienna, 1976), Report IRK 76/01; see also B. Strohmaier and M. Uhl, International Atomic Energy Agency Report IAEA-SMR-43, 1980, p. 313.
[12] O. Bersillon, in *Un programme de modele optique spherique* (Centre d'Etudes de Bruyères-le Châtel, Paris, 1981), Report CEA-N-2227.
[13] F. D. Becchetti and G. W. Greenlees, Phys. Rev. **182**, 1190 (1969).
[14] F. G. Perey, Phys. Rev. **131**, 745 (1962).
[15] L. McFadden and G. R. Satchler, Nucl. Phys. **84**, 177 (1966).
[16] Evaluated Nuclear Structure Data File (ENSDF) Database version of August 7, 2007, http://www.nndc.bnl.gov/ensdf/.
[17] W. Dilg, W. Schantl, H. Vonach, and M. Uhl, Nucl. Phys. **A217**, 269 (1973).
[18] V. Plyaskin and R. Kosilov, in *INDC(CCP)-424* (International Atomic Energy Agency, Vienna, 2000), p. 27.
[19] G. F. Steyn, C. Vermeulen, F. M. Nortier, F. Szelecsényi, Z. Kovács, and S. M. Qaim, Nucl. Instrum. Methods B **252**, 149 (2006).